Inorganic Chemistry

Article

pubs.acs.org/IC

Synthesis and Characterization of Two Quaternary Uranium Tellurides, $RbTiU_3Te_9$ and $CsTiU_3Te_9$

Matthew D. Ward,[†] Adel Mesbah,[†] Minseong Lee,[‡] Christos D. Malliakas,[†] Eun Sang Choi,[‡] and James A. Ibers*[,†]

[†]Department of Chemistry, Northwestern University, Evanston, Illinois 60208-3113, United States

[‡]Department of Physics and National High Magnetic Field Laboratory, Florida State University, Tallahassee, Florida 32310-3706, United States

Supporting Information

ABSTRACT: Black crystals of $RbTiU_3Te_9$ and $CsTiU_3Te_9$ have been synthesized at 1223 and 1173 K, respectively, by high-temperature solid-state routes. These compounds crystallize in a new structure type in space group C_{2h}^2-$P2_1/m$ of the monoclinic system. The structure, which is similar to that of $CsTiUTe_5$, consists of UTe_2 layers connected into a three-dimensional framework by $TiTe_6$ octahedra. The expanded UTe_2 layers leave channels that are filled by Rb or Cs atoms. Single-crystal resistivity measurements on $CsTiU_3Te_9$ are consistent with semiconducting behavior; the calculated activation energy is 0.30(1) eV. X-ray photoelectron spectroscopic measurements on $CsTiU_3Te_9$ indicate that the compound contains U^{4+}. From single-crystal magnetic measurements, $CsTiU_3Te_9$ is consistent with antiferromagnetic coupling between magnetic U atoms. The very low value of the effective magnetic moment of 0.56(2) μ_B is believed to arise from a coexistence of magnetic and nonmagnetic U atoms.

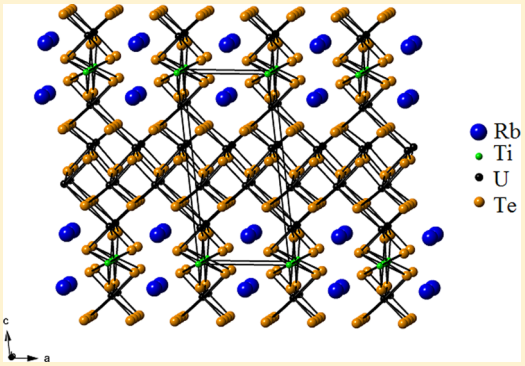

INTRODUCTION

Solid-state compounds of uranium, in particular, uranium chalcogenides, have been the subject of extensive research.[1] These compounds exhibit diverse magnetic properties because of the interactions of their f electrons. In particular, the binary uranium chalcogenides U_xQ_y have been well studied and show a range of magnetic properties, as exemplified by ferromagnetic UQ (Q = S, Se, Te),[2] paramagnetic UQ_3,[3] and antiferromagnetic U_2Te_3.[4]

Despite the extensive study of uranium chalcogenides, the number of sulfides and selenides far exceeds the number of uranium tellurides reported. The binary uranium tellurides typically are isostructural with the sulfides and selenides, although there exist some stoichiometries that are not observed with sulfur or selenium, such as UTe_5.[5,6] In general, the stability of metal binaries makes it difficult to synthesize more complex metal compounds. As a result, few ternary and even fewer quaternary uranium tellurides have been characterized. Ternary compounds that have been characterized as single crystals include MUTe (M = As, Sb),[7−9] $LnUTe_6$ (Ln = La, Ce, Pr, Nd, Sm, Gd),[10] $U_3Te_5Z_x$ (Z = Ge, Sn),[11] $Cu_{0.25}UTe_3$,[12] $Tl_{0.56}UTe_3$,[13] K_2UTe_3,[14] $Cu_{0.784}UTe_6$,[15] $CsUTe_6$,[16] and CsU_2Te_6.[17] Quaternary tellurides include $AAuUTe_3$ (A = Rb, Cs),[18] $Hg_3UTe_2Cl_6$,[19] $CsCuUTe_3$,[16] $CsMUTe_5$ (M = Ti, Zr),[16,20] $Cs_8Hf_5UTe_{30.6}$,[16] and $RbSb_{0.33}UTe_6$.[21]

Unlike uranium sulfides and most uranium selenides, the tellurides often display Te−Te interactions that are intermediate in length between $(Te-Te)^{2-}$ single bonds (2.76 Å)[22] and the $Te^{2-}\cdots Te^{2-}$ van del Waals distance (4.10 Å).[23] Such intermediate interactions can lead to new structures, but they make the assignment of formal oxidation states difficult.

Here we present the syntheses and structures of two new quaternary uranium tellurides, namely, $RbTiU_3Te_9$ and $CsTiU_3Te_9$, along with resistivity, X-ray photoelectron spectroscopy, and magnetic studies of $CsTiU_3Te_9$.

EXPERIMENTAL METHODS

Syntheses. The following reactants were used as received: Ti (Alfa 99.5%), Mn (Johnson Matthey 99.3%), Te (Aldrich 99.8%), Rb (Strem Chemicals 99+%), and CsCl (MP Biomedicals 99.9%). U powder was obtained through hydridization of depleted U turnings (Mfg. Sci. Corp.) followed by decomposition of the resultant hydride under vacuum.[9] Rb_2Te_3 flux was obtained by the stoichiometric reaction of Rb and Te in liquid NH_3 at 194 K.[24] The reactants were loaded into carbon-coated fused-silica tubes in an Ar-filled glovebox, evacuated to 10^{-4} Torr, and then flame sealed. Semiquantitative elemental analyses of the products were carried out with the use of a Hitachi S-3400 SEM equipped for EDX analysis.

Synthesis of $RbTiU_3Te_9$. With the ternary compound RbU_2Te_6 as the target, a mixture of U (30 mg, 0.216 mmol), Te (48.2 mg, 0.377 mmol), and Rb_2Te_3 (17.4 mg, 0.0314 mmol) was heated to 1223 K in 48 h, kept at 1223 K for 192 h, and cooled to 473 at 2 K h^{-1}, at which point the furnace was turned off. The reaction afforded black blocks in about 10 wt % yield. A few crystals were manually isolated. A crystal

Received: March 14, 2014
Published: July 22, 2014

   dx.doi.org/10.1021/ic500599d | Inorg. Chem. 2014, 53, 7909−7915

suitable for a single-crystal X-ray diffraction study was selected and analyzed by SEM-EDX to reveal the presence of Rb:Ti:U:Te in the approximate ratio 1:1:3:9. Subsequent analysis of the uranium turnings indicated that they were contaminated with about 10 wt % Ti. A rational synthesis involving Ti, U, and Te in a Rb_2Te_3 flux with the above heating profile failed to produce $RbTiU_3Te_9$.

Synthesis of $CsTiU_3Te_9$. Concurrently with the reaction that afforded $RbTiU_3Te_9$, a reaction of the Ti-contaminated U powder (0.030 g, 0.126 mmol), Mn (0.0069 g, 0.126 mmol), Te (0.0482 g, 0.378 mmol), and CsCl (0.1000 g, 0.594 mmol) was heated to 1173 K in 12 h, held at 1173 K for 6 h, cooled to 1073 K in 12 h, and held at this temperature for a further 96 h. The reaction was then cooled to 773 K over 60 h and finally cooled to 278 K in a further 12 h. Although the target was a U/Mn/Te compound, crystals of what turned out to be $CsTiU_3Te_9$ appeared as rectangular black plates. These plates were washed with water to remove excess flux and dried with acetone. They are stable for a day or two in air. Elemental analysis of the crystals revealed the presence of Cs, U, Te, and surprisingly Ti in an approximate ratio 1:3:9:1. No Mn was detected. Rational synthesis of the compound was achieved by replacing Mn with Ti in an equivalent molar amount and heating the reaction under the same heating profile as described above.

Structure Determinations. Single-crystal X-ray diffraction data were collected at 100(2) K on an APEX2 X-ray diffractometer equipped with graphite-monochromatized Mo Kα radiation.[25] The crystal-to-detector distance was 60 mm; the exposure time was 10 s/frame. Collection of intensity data, cell refinement, and data reduction were performed using APEX2 as a series of 0.3° scans in φ and ω.[25] Face-indexed absorption, incident beam, and decay corrections were performed by the program SADABS.[26] The structure of $RbTiU_3Te_9$ was solved and refined without difficulty with the use of the shelx-13 algorithms of the SHELXTL suite of programs.[27] However, solution and refinement of the $CsTiU_3Te_9$ structure presented an unusual problem. As described below, 4 of the 12 crystallographically independent atoms in the asymmetric unit are disordered in such a way as to form a major structure 89.7(1)% of the time and a minor structure 10.3(1)% of the time. The distribution of these structures appears to be random as the precession images prepared in APEX2 give no indication of long-range order or of a superstructure. Data collection on several crystals yielded the same results. Atom positions were standardized using the program STRUCTURE TIDY.[28] Crystallographic images were made using the program CRYSTALMAKER.[29] Further details are given in Table 1 and the Supporting Information.

Table 1. Crystallographic Data for $ATiU_3Te_9$ (A = Rb, Cs)[a]

compound	$RbTiU_3Te_9$	$CsTiU_3Te_9$
a/Å	8.216(1)	8.273(1)
b/Å	6.097(1)	6.115(1)
c/Å	17.407(1)	17.491(1)
V/Å^3	866.01(1)	878.71(1)
β/deg	96.733(4)	96.778(1)
$R(F)$ $[I > 2\sigma(I)]^b$	0.0307	0.0327
$R_w(F_o^2)^c$	0.0912	0.0814
q^d	0.0458	0.0222

[a]For both compounds: crystal system, monoclinc; space group, C_{2h}^2-$P2_1/m$; $Z = 2$; $T = 100(2)$ K. [b]$R(F) = \Sigma||F_o|-|F_c||/\Sigma|F_o|$ for $F_o^2 > 2\sigma(F_o^2)$. [c]$R_w(F_o^2) = \{\Sigma [w(F_o^2 - F_c^2)^2]/\Sigma wF_o^4\}^{1/2}$ for all data. [d]$w^{-1} = \sigma^2(F_o^2) + (qF_o^2)^2$ for $F_o^2 \geq 0$; $w^{-1} = \sigma^2(F_o^2)$ for $F_o^2 < 0$.

Resistivity. Two-probe resistivity data for $CsTiU_3Te_9$ were collected between 300 and 600 K using a homemade resistivity apparatus equipped with a Keithley 617 electrometer and a high-temperature vacuum chamber controlled by a K-20 MMR system. Data acquisition was controlled by custom-written software. Conductive silver (Dupont 4929N) was used for electrical contacts on the sample with Cu wire of 0.025 mm diameter (Omega). Single crystals with dimensions 0.38 mm × 0.35 mm × 0.21 mm (crystal 1) and 0.36 mm × 0.31 mm × 0.10 mm (crystal 2) were used for the measurements. Direct current was applied along an arbitrary direction parallel to the Ti planes for crystal 1 and parallel and normal to the Ti planes for crystal 2.

X-ray Photoelectron Spectroscopy. X-ray photoelectron spectra of $CsTiU_3Te_9$ were measured on a Thermo Scientific ESCALAB 250Xi spectrometer with a vacuum of 1.0×10^{-9} mbar at 298 K. Several crystals of $CsTiU_3Te_9$ that had grown together were placed on a Cu backing tape for analysis. Binding energies of electrons E_b (eV) in all spectra were calibrated by setting the aliphatic C 1s peak to 285 eV.

Magnetic Susceptibility Measurement. Magnetic susceptibility was measured on a Quantum Design MPMS SQUID magnetometer between 2 and 300 K on a 5.9 mg sample of $CsTiU_3Te_9$ prepared by grinding single crystals. The sample was placed in a gelatin capsule. Data were taken under zero-field-cooled (ZFC) or field-cooled (FC) conditions at fields of 1, 6, 10, and 70 kOe. FC and ZFC data are practically identical.

RESULTS AND DISCUSSION

Synthesis. $RbTiU_3Te_9$ was synthesized from reaction of Ti-contaminated U and Te in an Rb_2Te_3 flux at 1223 K in a yield of about 10 wt %. A rational synthesis involving U, Ti, and Te failed to produce $RbTiU_3Te_9$.

$CsTiU_3Te_9$ was initially obtained from reaction of Ti-contaminated U, Mn, and Te in a CsCl flux at 1173 K in a yield of about 50 wt % based on U. A rational synthesis in which the Mn was replaced with an equivalent molar amount of Ti was successful. The yield of $CsTiU_3Te_9$ from this rational reaction was about 90 wt % based on U. All reactions yielded black plates or blocks of the title compounds as well as U/Te binaries and excess flux.

Crystal Structure of $RbTiU_3Te_9$. $RbTiU_3Te_9$ crystallizes in a new structure type with two formula units in the monoclinic space group C_{2h}^2-$P2_1/m$. The asymmetric unit contains one Rb, one Ti, three U, and seven Te crystallographically independent atoms. Their site symmetries are Ti($\bar{1}$), Te1(1), and Te2(1) and all the others m.

The structure of $RbTiU_3Te_9$ consists of UTe_2 layers connected into a three-dimensional framework by $TiTe_6$ octahedra (Figure 1). The structure is similar to that of $CsTiUTe_5$,[16] except that the UTe_2 layers have been expanded (Figure 2). This creates a three-dimensional framework with channels rather than infinite sheets as in $CsTiUTe_5$.[16] The UTe_2 layers are composed of three crystallographically independent U atoms and seven Te atoms. U atoms are

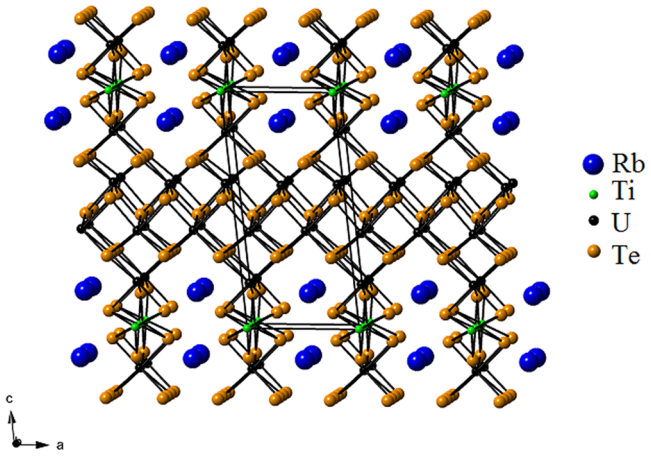

Figure 1. Structure of $RbTiU_3Te_9$.

dx.doi.org/10.1021/ic500599d | Inorg. Chem. 2014, 53, 7909−7915

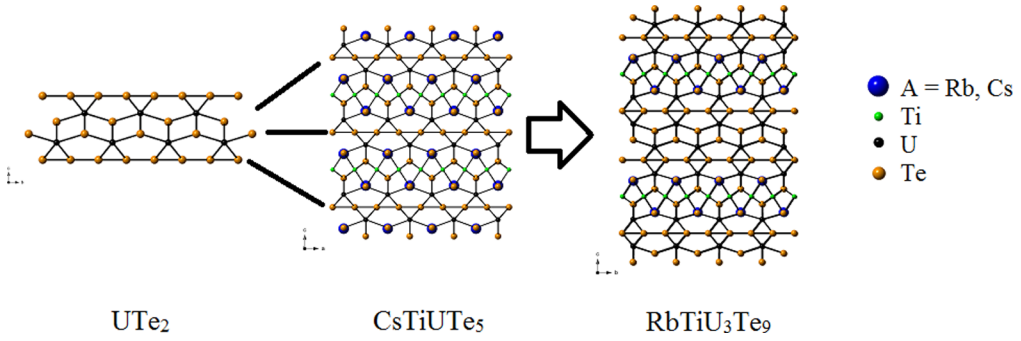

Figure 2. Relationship among UTe_2,[30] $CsTiUTe_5$,[16] and $RbTiU_3Te_9$.

coordinated by eight Te atoms in a bicapped trigonal-prismatic arrangement. Te1 and Te2 atoms each form infinite Te−Te−Te chains in the [010] direction on the uncapped faces of the bicapped trigonal prisms. The centers of the UTe_2 layers are composed of U2 atoms and U3 atoms that share three Te atoms (Te1, Te2, and Te6) of the triangular faces in the [100] direction to form infinite chains. These chains then form infinite sheets by sharing the capping Te atoms and the Te atoms of the capped edges. At the edges of the UTe_2 layers the U1 atoms share the Te atoms of the uncapped faces to form square-based biprisms with the U2 atom as seen in the structure of UTe_2[30] (Figure 3). UTe_2 layers are disrupted from

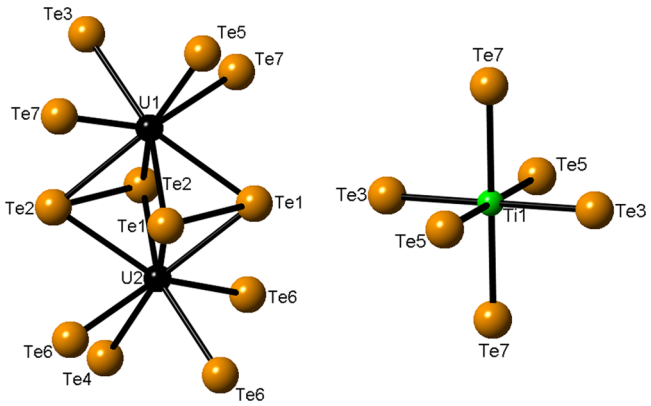

Figure 3. Uranium biprism (a) and titanium octahedron (b) formed within the U/Te layer of $RbTiU_3Te_9$.

continuing to stack by insertion of Ti atoms. These coordinate to form octahedra with the remaining Te atoms (Te3, Te5, Te7) that the U1 atoms do not share with the U2 atoms. Each Ti atom coordinates to three Te atoms from two UTe_2 layers to form $TiTe_6$ octahedra (Figure 3) that reside between the UTe_2 layers. The disruption of the UTe_2 structure by these $TiTe_6$ octahedra creates channels along [010] within which the Rb atoms reside.

The U−Te interatomic distances in $RbTiU_3Te_9$ (Table 2) compare favorably with those seen in UTe_2.[30] UTe_2 has U−Te distances that range from 3.078(1) to 3.199(1) Å at 118 K, whereas the U−Te distances in $RbTiU_3Te_9$ range from 3.000(1) to 3.194(1) Å for U1−Te, 3.048(1) to 3.202(1) Å for U2−Te, and 3.071(1) to 3.216(1) Å for U3−Te at 100 K. Ti−Te distances range from 2.804(1) to 2.807(1) Å compared with those in $CsTiUTe_5$ of 2.787(1) and 2.788(1) Å.[16]

Crystal Structure of $CsTiU_3Te_9$. $CsTiU_3Te_9$ also crystallizes with two formula units in the monoclinic space group C_{2h}^2-$P2_1/m$. The asymmetric unit contains two Cs, two Ti, four U,

Table 2. Selected Interatomic Distances (Angstroms)[a] for $RbTiU_3Te_9$

U1−Te3	3.000(1)	U3−Te6	3.071(1)
U1−Te5	3.001(1)	U3−Te4	3.096(1)
U1−Te7 × 2	3.171(1)	U3−Te2 × 2	3.140(1)
U1−Te1 × 2	3.194(1)	U3−Te1 × 2	3.140(1)
U1−Te2 × 2	3.194(1)	U3−Te4 × 2	3.216(1)
U1−Ti1 × 2	3.569(1)	Te1−Te1	3.048(1)
U1−U2	3.817(1)	Te1−Te1	3.049(1)
U2−Te6	3.048(1)	Te2−Te2	3.046(1)
U2−Te4	3.070(1)	Te2−Te2	3.051(1)
U2−Te2 × 2	3.141(1)	Ti1−Te7 × 2	2.804(1)
U2−Te1 × 2	3.142 (1)	Ti1−Te3 × 2	2.806(1)
U2−Te6 × 2	3.202(1)	Ti1−Te5 × 2	2.807(1)
U2−U3	4.097(1)	Ti1−Ti1 × 2	3.049(1)
U2−U3	4.121(1)		

[a]All interatomic distances have been rounded to three significant figures.

and eight Te crystallographically independent sites. The extra sites compared with those in $RbTiU_3Te_9$ arise because of disorder. Their site symmetries are all *m* except Ti1 ($\bar{1}$), Ti1a ($\bar{1}$), Te1 (1), and Te2 (1), where the disordered sites have been labeled Cs1a, Ti1a, U1a, and Te7a.

The structure of $CsTiU_3Te_9$ closely resembles that of $RbTiU_3Te_9$. The central UTe_2 layers are identical to those in $RbTiU_3Te_9$, but the edges of these layers and the Ti layers are more complicated because of disorder in the U1, Ti1, Cs1, and Te7 sites. In the $RbTiU_3Te_9$ structure, the U1 atom only shares the Te1 and Te2 atoms to form biprisms with atom U2. However, in the $CsTiU_3Te_9$ structure, the U1 atom shares the infinite Te1 and Te2 chains to form biprisms with either the U2 or the U3 atoms in a disordered fashion. The U1 atom forms biprisms with the U2 atom 89.7(1)% of the time, and the U1a atom forms biprisms with the U3 the remaining 10.3(1)% of the time. The position of U1 determines where Te7, Ti1, and Cs1 are, and the position of U1a determines where Te7a, Ti1a, and Cs1a are so as to maintain the structure shown in Figure 4. Another way to understand this disorder is to note that the left and right drawings in Figure 4 are related by a shift of 1/2 *a*.

The U−Te interatomic distances in $CsTiU_3Te_9$ (Table 3) again compare favorably with those in UTe_2.[30] The U−Te distances in $CsTiU_3Te_9$ range from 2.966(3) to 3.276(3) Å for U1−Te, 2.994(1) to 3.216(1) Å for U1a−Te, 3.077(1) to 3.226(1) Å for U2−Te, and 3.054(1) to 3.212(1) Å for U3−Te. Note that the U1a−Te1 and U1a−Te2 distances are noticeably shorter than those seen for the more prevalent U1 site. This causes the U1a site to be closer to the UTe_2 layers

dx.doi.org/10.1021/ic500599d | Inorg. Chem. 2014, 53, 7909−7915

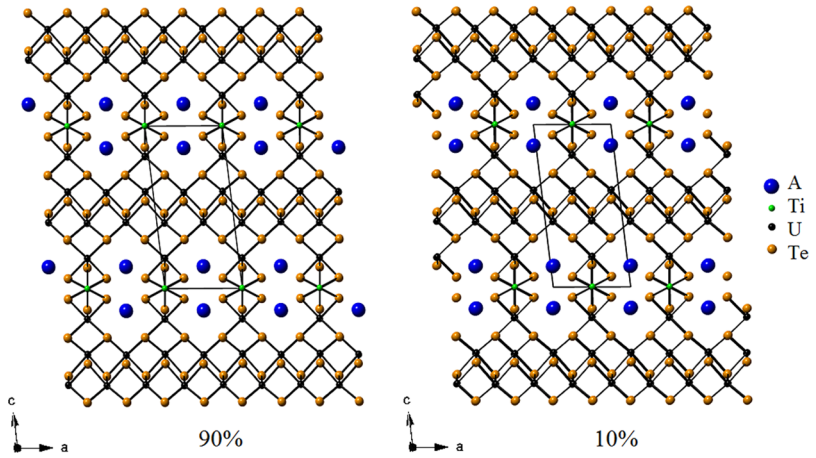

Figure 4. Disorder between the U/Te layers in $CsTiU_3Te_9$.

Table 3. Selected Interatomic Distances (Angstroms)[a] for $CsTiU_3Te_9$

U1−Te3	2.966(3)	U2−U3	4.150(1)
U1−Te5	2.978(3)	U3−Te4	3.054(1)
U1−Te7 × 2	3.212(1)	U3−Te6	3.077(1)
U1−Te1 × 2	3.275(3)	U3−Te2 × 2	3.143(1)
U1−Te2 × 2	3.276(3)	U3−Te1 × 2	3.143(1)
U1−Ti1 × 2	3.586(3)	U3−Te4 × 2	3.212(1)
U1−U2	3.753(1)	Te1−Te1	3.052(1)
U1a−Te3	2.994(1)	Te1−Te1	3.063(1)
U1a−Te5	2.996(1)	Te2−Te2	3.051(1)
U1a−Te7a[b] × 2	3.184(1)	Te2−Te2	3.064(1)
U1a−Te1 × 2	3.216(1)	Ti1−Te3 × 2	2.786(1)
U1a−Te2 × 2	3.216(1)	Ti1a−Te3 × 2	2.806(1)
U1a−Ti1a × 2	3.592(1)	Ti1−Te5 × 2	2.788(1)
U2−Te4	3.077(1)	Ti1a−Te5 × 2	2.806(1)
U2−Te6	3.103(1)	Ti1−Te7 × 2	2.728(1)
U2−Te2 × 2	3.147(1)	Ti1a−Te7a × 2	2.813(1)
U2−Te1 × 2	3.150(1)	Ti1−Ti1 × 2	3.058(1)
U2−Te6 × 2	3.226(1)	Ti1a−Ti1a × 2	3.058(1)
U2−U3	4.125(1)		

[a]All interatomic distances have been rounded to three significant figures. [b]The disordered atoms in the minor component are labeled with an "a".

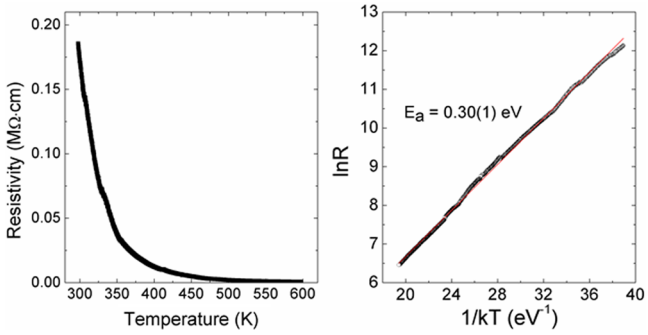

Figure 5. Temperature-dependent resistivity (ρ) and the corresponding Arrhenius plot for $CsTiU_3Te_9$.

than is the U1 site. Consequently, the U1a−Te3 and U1a−Te5 distances are longer than the corresponding U1 distances. The Ti1−Te distances range from 2.728(1) to 2.788(1) Å, and the Ti1a−Te distances range from 2.806(1) to 2.813(1) Å.

Resistivity. Figure 5 shows that the resistivity of crystal 1 of $CsTiU_3Te_9$ decreases from 0.18 MΩ·cm at 300 K to 0.6 kΩ·cm at 600 K, consistent with semiconducting behavior. The corresponding calculated activation energy is 0.30(1) eV, and the Arrhenius plot (Figure 5) is linear, indicative of a single carrier excitation mechanism. We attribute the small discontinuities in the plots shown in Figure 5 to instrumental artifacts resulting from contact instability on the surface of the small crystal at high temperature. Conductivity measurements on crystal 2 (Supporting Information) suggest that $CsTiU_3Te_9$ is a semiconductor both normal and parallel to the Ti planes. The calculated activation energies are 0.15(1) eV along the normal direction and 0.05(1) eV along the parallel direction. These values for crystal 2 are lower than that for crystal 1, perhaps because of crystal instability or to the different degree of disorder in each single crystal.

X-ray Photoelectron Spectroscopy. The binding energies for the U $4f_{7/2}$ and $4f_{5/2}$ peaks of $CsTiU_3Te_9$ occur at 381.81 and 392.67 eV, respectively. The spectrum is shown in Figure 6. The U $4f_{7/2}$ binding energy observed for $CsTiU_3Te_9$ is consistent with that of 381.30 eV for UTe_3.[31] Other reported binding energies for uranium tellurides include U_2Te_3 and U_3Te_4, which have $4f_{7/2}$ binding energies of 380.7 and 380.5 eV, respectively.[31] UTe_3 structurally contains a ditelluride Te_2 group and charge balances as $U^{4+}(Te_2^{2-})Te^{2-}$. Because the binding energies of UTe_3 and $CsTiU_3Te_9$ differ so little we believe that $CsTiU_3Te_9$ contains U^{4+}. Even with this assignment, rational charge balance of the $RbTiU_3Te_9$ and $CsTiU_3Te_9$ compounds is still ambiguous owing to the intermediate Te−Te distances in their infinite Te−Te−Te chains. It is interesting that the binding energy of 381.81 eV in $CsTiU_3Te_9$ is also consistent with those in several U^{4+} oxides.[32]

Oxidation State. A proposed model for charge balance is as follows: Cs^{1+}, Ti^{2+}, 3 × U^{4+}, 5 × Te^{2-}, resulting in an overall charge of 5+ that must balanced by the four remaining Te atoms belonging to the Te−Te−Te infinite chains. This results in an average charge of −1.25 e^- on those atoms. There is precedent for Ti^{2+}, for example, in U_8TiQ_{17} (Q = S, Se),[33,34] as well as for an average charge of −1.25 e^- per Te in infinite linear Te−Te−Te chains, as observed in the AAn_2Q_6 family.[35,36] A noninteger average charge for Te is also found in a number of compounds with Te square-net sheets.[37]

Magnetic Susceptibility. Given the lack of sufficient $RbTiU_3Te_9$, magnetic measurements were restricted to

dx.doi.org/10.1021/ic500599d | Inorg. Chem. 2014, 53, 7909−7915

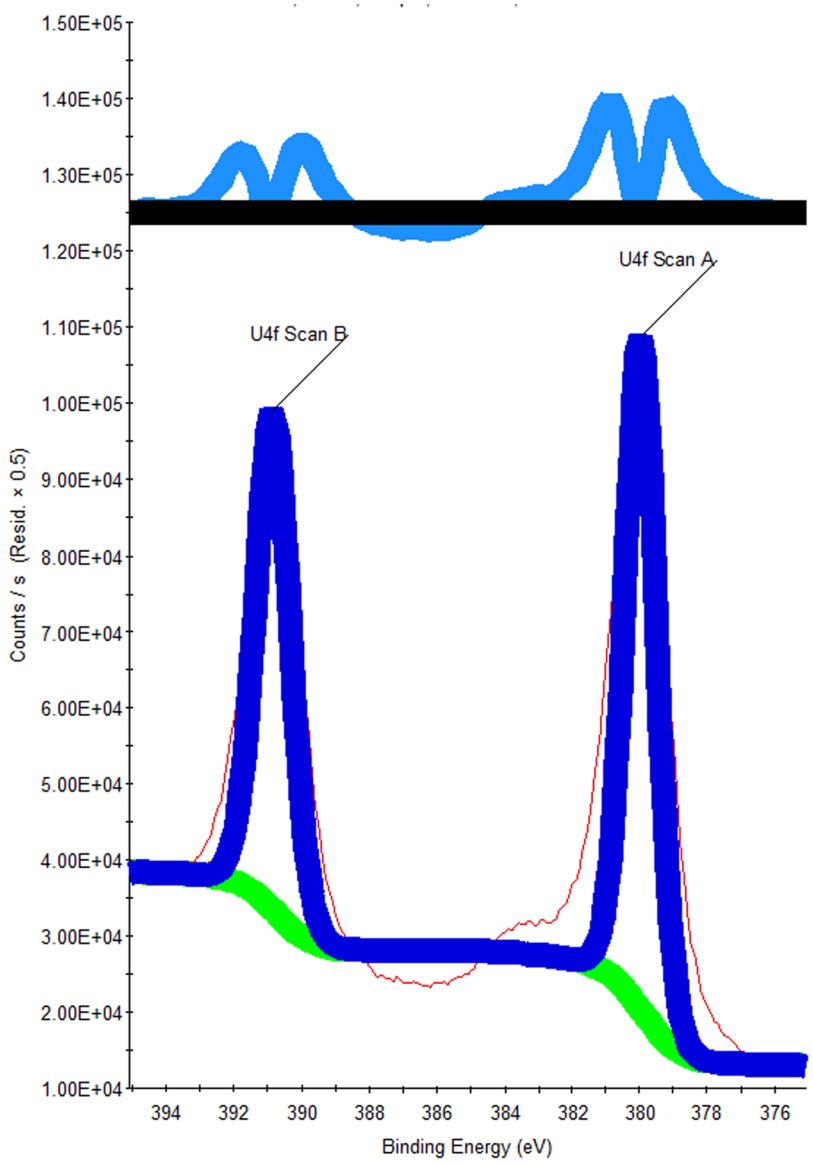

Figure 6. U $4f_{7/2}$ and U $4f_{5/2}$ peaks in the X-ray photoelectron spectrum of $CsTiU_3Te_9$.

$CsTiU_3Te_9$. Figure 7a shows the temperature dependence of the magnetic moment (m) taken at different fields and the magnetic susceptibility ($\chi = m/H$) of $CsTiU_3Te_9$ at 6 kOe. In the entire measured temperature range (2 K $\leq T \leq$ 300 K), the temperature dependence does not show monotonic behavior but rather shows a broad minimum around 100 K. The origin of the abnormal temperature dependence is not understood. It cannot arise from the sample holder as its background measured separately shows temperature-independent diamagnetism. On the other hand, $\chi(T)$ follows the modified Curie–Weiss law at temperatures below 80 K without any signature of a phase transition down to 2 K.

We restrict our discussion to the low-temperature data only. The modified Curie–Weiss law can be expressed as $\chi = C/(T - \theta) + \chi_0$, where C is the Curie constant, χ_0 is the temperature-independent susceptibility, and θ is the Weiss temperature. Fitting parameters were obtained by plotting the inverse magnetic susceptibility $1/(\chi - \chi_0)$ as a function of temperature, as shown in Figure 7b. The effective magnetic moment (μ_{eff}) is 0.56(2) μ_B per U atom as obtained from the relation $\mu_{eff} = (7.997C)^{1/2}$. θ is estimated to be −1.9(1) K, which suggests antiferromagnetic coupling between magnetic ions. χ_0 is fitted to be positive with values of ~1.7(1) × 10^{-3} emu mol^{-1}, which in general could be caused by Pauli paramagnetism from itinerant electrons or small ferromagnetic impurities. However, the electric resistance measurements revealed semiconducting behavior (see Figure 5) with an activation energy of 0.30(1) eV, which excludes the possibility of Pauli paramagnetism. The possibility of a ferromagnetic impurity (for example, UTe[38] (T_c ≈ 120 K)) cannot be excluded, because a minor amount would not be detected by X-ray powder diffraction measurements. The μ_{eff} value of 0.56 μ_B is much smaller than those for free-ion moments of U^{3+} (3.62 μ_B) or U^{4+} (3.58 μ_B) with L–S coupling. Reduced effective moments in actinides are not unusual and often are attributed to the crystalline electric field (CEF) effect or to itinerant 5f electrons. However, it is difficult to expect a reduction of μ_{eff} by more than 80% by either effect,[39] particularly because itinerant magnetism is not relevant here and the low local symmetry of the U atoms should reduce the CEF effect.

An alternative scenario is a coexistence of magnetic and nonmagnetic U atoms. Within the CEF model, two 5f electrons

dx.doi.org/10.1021/ic500599d | Inorg. Chem. 2014, 53, 7909–7915

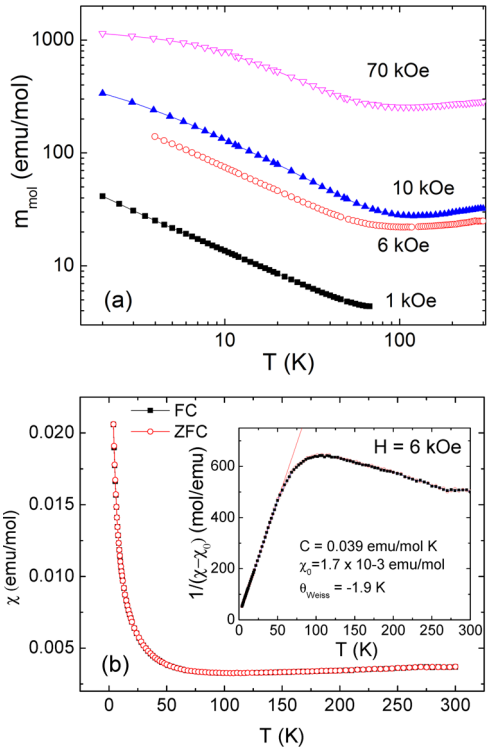

Figure 7. Temperature dependence of the molar magnetic moment (m) at different fields (a), and ZFC and FC magnetic susceptibility (χ) of $CsTiU_3Te_9$ for H= 6 kOe (b). (Inset) Inverse magnetic susceptibility.

can occupy the same CEF level and result in a nonmagnetic single ground state. Thus, U^{2+} ($5f^4$) or U^{4+} ($5f^2$) can have such a singlet ground state, as observed experimentally.[40] In general, the singlet ground state can manifest itself from bulk magnetic property measurements when the energy scale of the temperature (k_BT) or magnetic field (μ_BH) is varied across the singlet−triplet energy gap (i.e., $k_BT \approx \Delta$ or $\mu_BH \approx \Delta$, respectively, where k_B is the Boltzmann constant, μ_B is the Bohr magneton, and Δ is the energy gap between the singlet and the lowest lying triplet state). However, in our case, the presumed existence of magnetic ions could hinder the observation of such a transition.

X-ray photoelectron spectroscopic results support the U^{4+} oxidation state, which satisfies the necessary condition to have a spin-singlet state. It is therefore reasonable that the majority of U^{4+} atoms are in the spin-singlet ground state, whereas the minority are responsible for the observed magnetic behavior. Note that the U1−U2 distance of 3.753(1) Å is close to the Hill limit of magnetic ordering. Measurements below the Weiss temperature (1.9(1) K)) could be used to determine the disposition of U atoms between the magnetic and the nonmagnetic ground states.

Figure 8 shows the magnetization data taken at 2 and 5 K. The magnetization follows simple paramagnetic behavior with no sign of hysteresis and is far from saturation in the measured field range. Magnetization measurements at much higher fields would examine the proposed singlet ground state, because a sudden jump of magnetization should occur when the external field is comparable with the singlet−triplet energy gap.

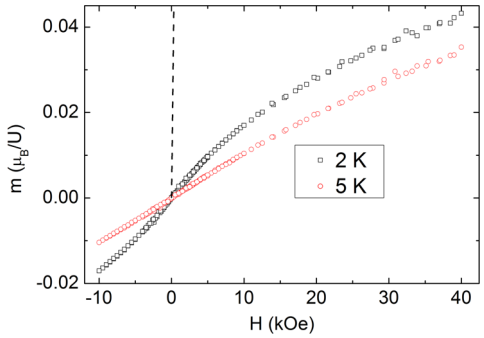

Figure 8. Magnetization data (m) of $CsTiU_3Te_9$ at T = 2 and 5 K. Both up and down sweeps are shown. Dashed line is the Brillouin function for free U^{4+} ion for T = 2 K.

CONCLUSIONS

Black crystals of $RbTiU_3Te_9$ and $CsTiU_3Te_9$ crystallize in a new structure type in space group C_{2h}^2-$P2_1/m$ of the monoclinic system. The structure, which is nearly identical to that of $CsTiUTe_5$, consists of UTe_2 layers connected into a three-dimensional framework by $TiTe_6$ octahedra. The expanded UTe_2 layers leave channels that are filled by Rb or Cs atoms. Single-crystal resistivity measurements on $CsTiU_3Te_9$ are consistent with semiconducting behavior; the calculated activation energy is 0.30(1) eV. X-ray photoelectron spectroscopic measurements on $CsTiU_3Te_9$ support a U^{4+} oxidation state. From magnetic measurements, $CsTiU_3Te_9$ is consistent with antiferromagnetic coupling between magnetic U atoms. The effective magnetic moment of 0.56(2) μ_B is very low. It is believed to arise from a coexistence of magnetic and nonmagnetic U atoms, with the majority of the U^{4+} atoms in the spin-singlet ground state whereas the minority are responsible for the observed magnetic behavior. The shortest U−U distance of 3.753(1) Å is close to the Hill limit of magnetic ordering.

ASSOCIATED CONTENT

Supporting Information

Crystallographic files in cif format for $RbTiU_3Te_9$ and $CsTiU_3Te_9$, and resistivity measurements on crystal 2. This material is available free of charge via the Internet at http://pubs.acs.org.

AUTHOR INFORMATION

Corresponding Author

*E-mail: ibers@chem.northwestern.edu.

Notes

The authors declare no competing financial interest.

ACKNOWLEDGMENTS

This research was kindly supported at Northwestern University by the U.S. Department of Energy, Basic Energy Sciences, Chemical Sciences, Biosciences, and Geosciences Division and Division of Materials Science and Engineering Grant ER-15522. Use was made of the IMSERC X-ray Facility at Northwestern University, supported by the International Institute of Nanotechnology (IIN). A portion of this work was performed at the National High Magnetic Field Laboratory, which is supported by NSF Cooperative Agreement No. DMR-1157490, by the State of Florida, and by the DOE.

REFERENCES

(1) Grenthe, I.; Drozdzynski, J.; Fujino, T.; Buck, E. C.; Albrecht-Schmitt, T. E.; Wolf, S. F. In *The Chemistry of the Actinide and Transactinide Elements*, 4th ed.; Morss, L. R., Edelstein, N. M., Fuger, J., Eds.; Springer: Dordrecht, 2011; Vol. *1*, pp 253−698.
(2) Busch, G.; Vogt, O.; Delapalme, A.; Lander, G. H. *J. Phys. C: Solid State Phys.* **1979**, *12*, 1391−1401.
(3) Noël, H. *J. Less-Common Met.* **1986**, *121*, 265−270.
(4) Suski, W.; Wojakowski, A.; Blaise, A.; Salmon, P.; Fournier, J. M.; Mydlarz, T. *J. Magn. Magn. Mater.* **1976**, *3*, 195−200.
(5) Noël, H. *Mater. Res. Bull.* **1984**, *19*, 1171−1175.
(6) Noël, H. *Inorg. Chim. Acta* **1985**, *109*, 205−207.
(7) Pietraszko, D.; Lukaszewicz, K. *Bull. Acad. Polym. Sci., Ser. Sci. Chim.* **1975**, *23*, 337−340.
(8) Hulliger, F. *J. Less-Common Met.* **1968**, *16*, 113−117.
(9) Haneveld, A. J. K.; Jellinek, F. *J. Less-Common Met.* **1969**, *18*, 123−129.
(10) Slovyanskikh, V. K.; Kuznetsov, N. T. *Russ. J. Inorg. Chem. (Transl. of Zh. Neorg. Khim.)* **1990**, *35*, 447.
(11) Tougait, O.; Potel, M.; Noël, H. *J. Solid State Chem.* **2002**, *168*, 217−223.
(12) Patschke, R.; Breshears, J. D.; Brazis, P.; Kannewurf, C. R.; Billinge, S. J. L.; Kanatzidis, M. G. *J. Am. Chem. Soc.* **2001**, *123*, 4755−4762.
(13) Tougait, O.; Daoudi, A.; Potel, M.; Noël, H. *Mater. Res. Bull.* **1997**, *32*, 1239−1245.
(14) Stöwe, K.; Appel-Colbus, S. *Z. Anorg. Allg. Chem.* **1999**, *625*, 1647−1651.
(15) Huang, F. Q.; Ibers, J. A. *J. Solid State Chem.* **2001**, *159*, 186−190.
(16) Cody, J. A.; Ibers, J. A. *Inorg. Chem.* **1995**, *34*, 3165−3172.
(17) Mesbah, A.; Ibers, J. A. *Acta Crystallogr., Sect. E: Struct. Rep. Online* **2012**, *68*, i76.
(18) Bugaris, D. E.; Ibers, J. A. *J. Solid State Chem.* **2009**, *182*, 2587−2590.
(19) Bugaris, D. E.; Ibers, J. A. *J. Solid State Chem.* **2008**, *181*, 3189−3193.
(20) Kim, J.-Y.; Gray, D. L.; Ibers, J. A. *Acta Crystallogr., Sect. E: Struct. Rep. Online* **2006**, *E62*, i124−i125.
(21) Choi, K. S.; Kanatzidis, M. G. *J. Solid State Chem.* **2001**, *161*, 17−22.
(22) Brattås, L.; Kjekshus, A. *Acta Chem. Scand.* **1972**, *26*, 3441−3449.
(23) Shannon, R. D. *Acta Crystallogr., Sect. A: Cryst. Phys., Diffr., Theor. Gen. Crystallogr.* **1976**, *32*, 751−767.
(24) Klemm, V. W.; Sodomann, H.; Langmesser, P. *Z. Anorg. Allg. Chem.* **1939**, *241*, 281−304.
(25) *Bruker APEX2 Version 2009.5-1 and SAINT version 7.34a Data Collection and Processing Software*; Bruker Analytical X-Ray Instruments, Inc.: Madison, WI, USA, 2009.
(26) Sheldrick, G. M. *SADABS; Department of Structural Chemistry*; University of Göttingen: Göttingen, Germany, 2008.
(27) Sheldrick, G. M. *Acta Crystallogr., Sect. A: Found. Crystallogr.* **2008**, *64*, 112−122.
(28) Gelato, L. M.; Parthé, E. *J. Appl. Crystallogr.* **1987**, *20*, 139−143.
(29) Palmer, D. *CrystalMaker Software*, Version 2.7.7; CrystalMaker Software Ltd.: Oxford, England, 2013.
(30) Stöwe, K. *J. Solid State Chem.* **1996**, *127*, 202−210.
(31) Sergushin, N. P.; Nefedov, V. I.; Rozanov, I. A.; Slovyanskikh, V. K.; Gracheva, N. V. *Russ. J. Inorg. Chem. (Transl. of Zh. Neorg. Khim.)* **1977**, *22*, 856−858.
(32) Teterin, Y. A.; Utkin, I. O.; Melnikov, I. V.; Lebedev, A. M.; Teterin, A. Y.; Ivanov, K. E.; Nikitin, A. S.; Vukchevich, L. *J. Struct. Chem. (Engl. Trans.)* **2000**, *41*, 965−971.
(33) Noël, H. *C. R. Seances Acad. Sci., Ser. C* **1973**, *277*, 463−464.
(34) Noël, H. *C. R. Seances Acad. Sci., Ser. C* **1974**, *279*, 513−515.
(35) Choi, K.-S.; Patschke, R.; Billinge, S. J. L.; Waner, M. J.; Dantus, M.; Kanatzidis, M. G. *J. Am. Chem. Soc.* **1998**, *120*, 10706−10714.
(36) Bugaris, D. E.; Wells, D. M.; Yao, J.; Skanthakumar, S.; Haire, R. G.; Soderholm, L.; Ibers, J. A. *Inorg. Chem.* **2010**, *49*, 8381−8388.
(37) Patschke, R.; Kanatzidis, M. G. *Phys. Chem. Chem. Phys.* **2002**, *4*, 3266−3281.
(38) Suski, W.; Mydlarz, T.; Rao, V. U. S. *Phys. Status Solidi A* **1972**, *14*, K157−K160.
(39) Sechovsky, V.; Havela, L. In *Handbook of Magnetic Materials*, 1st ed.; Buschow, K. H. J., Ed.; Elsevier: Amsterdam, 1998; Vol. *11*, pp 1−290.
(40) Cooper, B. R.; Vogt, O. *J. Phys. Colloq.* **1979**, *C4*, 66−67.